SECOND YEAR REPORT OF AOARD-07-4014 CONTRACT (2008.07.01-2009.05.17)

Polymer-Nanoparticle Hybrid Photovoltaic Research for U.S. Air Force Applications

PI: Wei-Fang Su, suwf@ntu.edu.tw, **Co-PI:** Chun-Wei Chen, chunwei@ntu.edu.tw
Department of Materials Science and Engineering, National Taiwan University,
1, Roosevelt Road, Sec 4, Taipei, Taiwan,
+886-2-3366-4078 (phone), +886-2-2363-4562 (fax)

Abstract

The polymer photovoltaic devices based on the poly(3-hexylthiophene)/TiO_2 nanorods hybrid material (P3HT/TiO_2) has better thermal stability than that of P3HT/PCBM hybrid material. We have investigated the effect of polymer molecular weight on the morphology and performance of P3HT/TiO_2 nanorod hybrid photovoltaic devices by using scanning near field optical microscopy (SNOM), atomic force microscopy (AFM) and confocal Raman microscopy. The results provide a direct observation of the correlation between the nanoscale absorption, morphology and device performance. An enhancement in the device performance can be achieved by removing or replacing the insulating surfactant on the TiO_2 nanorods surface with a more conductive ligand, which can play the role to assist charge separation efficiency or also to prevent from back recombination, giving a large improvement in the short circuit current and fill factor. The F-doped TiO_2 nanocrystal has increased the carrier concentration, conductivity and charge separation efficiency of the hybrid that results improved power conversion efficiency. A novel series of soluble alternating conjugated copolymers, comprised of 9,9-dihexylfluorene and cyclopentadithiophenes (**P1**-**P5**), were synthesized via Pd-catalyzed Suzuki coupling reaction in good yields. The **P2** and **P3** with electron donating non-π-substituents (ethylenedioxy and propylenedioxy bridges the 3,3 positions of the thiophene groups) display high fluorescence quantum yields and red-shifted absorption as compared with non substituted **P1**. However, the **P4** and **P5** are weakly fluorescent and exhibit blue-shifted absorption which are due to the presence of electron-withdrawing π-substituents (carbonyl and dicyanoethenyl). Their applications in the photovoltaic device are current under investigation.

Report Documentation Page

Form Approved
OMB No. 0704-0188

1. REPORT DATE	2. REPORT TYPE	3. DATES COVERED
06 JAN 2010	**FInal**	**18-05-2007 to 17-05-2009**

4. TITLE AND SUBTITLE
Nanocolumn Structure with Branches Hybrid Photovoltaic Research for Space Applications

5a. CONTRACT NUMBER
FA48690714014

5b. GRANT NUMBER

5c. PROGRAM ELEMENT NUMBER

6. AUTHOR(S)
Wei-Fang Su

5d. PROJECT NUMBER

5e. TASK NUMBER

5f. WORK UNIT NUMBER

7. PERFORMING ORGANIZATION NAME(S) AND ADDRESS(ES)
National Taiwan University,1, Roosevelt Road Sec. 4,Taipei 106,Taiwan,TW,106

8. PERFORMING ORGANIZATION REPORT NUMBER
N/A

9. SPONSORING/MONITORING AGENCY NAME(S) AND ADDRESS(ES)
AOARD, UNIT 45002, APO, AP, 96337-5002

10. SPONSOR/MONITOR'S ACRONYM(S)
AOARD

11. SPONSOR/MONITOR'S REPORT NUMBER(S)
AOARD-074014

12. DISTRIBUTION/AVAILABILITY STATEMENT
Approved for public release; distribution unlimited

13. SUPPLEMENTARY NOTES

14. ABSTRACT
This is a project concerned with polymer photovoltaic devices based on poly(3-hexylthiophene)/TiO2 nanorod hybrids.

15. SUBJECT TERMS
Solar Cells, Polymer Chemistry

16. SECURITY CLASSIFICATION OF:			17. LIMITATION OF ABSTRACT	18. NUMBER OF PAGES	19a. NAME OF RESPONSIBLE PERSON
a. REPORT	b. ABSTRACT	c. THIS PAGE			
unclassified	**unclassified**	**unclassified**	**Same as Report (SAR)**	**22**	

Introduction

Recently, hybrids of organic polymers and inorganic nanocrystals have attracted a great of interest due to their potential application in developing the low-cost, large-area, mechanically flexible photovoltaic devices.[1,2] A basic requirement for a photovoltaic material is to generate free charge carriers produced by photoexcitation. Subsequently, these carriers are transported through the device to the electrodes without recombining with oppositely charged carriers. Due to the low dielectric constant of organic materials, the dominant photogenerated species in most conjugated polymer is a neutral bound electron–hole pair (exciton). These neutral excitons can be dissociated from Coulomb attraction by offering an energetically favorable pathway for the electron from polymer (donor) to transfer onto an electron-accepting specie (acceptor). Because the diffusion length of excitons in a semiconducting polymer is usually shorter than 20 nm, [3-5] the electron acceptor must be intermixed with polymer at a nanometer length scale to achieve efficient charge separation. The most commonly used structure is the polymer-based bulk heterojunction (BHJ) solar cell, which consists of the electron accepting network formed randomly within the polymer matrix. The most popular electron acceptors in the BHJ polymer photovoltaic devices are C_{60} derivatives (PCBM)[6,7] and nanocrystals such as CdSe[1,8] or TiO_2.[9-11] After charge separation, electrons and holes must be transported to the opposite electrode before back recombination occurs. Then, the current is generated. We have been focused on the development of polymer-TiO_2 photovoltaic device, because the TiO_2 is nontoxic, thermal stable and low cost. For the second year of this program, we have investigated the effect of polymer molecular weight on the morphology and performance of poly(3-hexylthiophene)/TiO_2 nanorod hybrid photovoltaic devices . We have studied various conducting ligands to modify the TiO_2 surface, synthesized new F-doped TiO_2 nanorods and new fluorene-cyclopentadithiophene conducting copolymers to improve the power conversion efficiency of photovoltaic devices.

Results and discussion

Nanoscale morphology and performance of molecular-weight-dependent poly(3-hexylthiophene)/TiO2 nanorod hybrid solar cells[12,13]

Figure 1 shows the absorption spectra of P3HT/TiO_2 nanorod hybrid thin films (50 : 50 wt%) with different polymer MWs. A redshift in the absorption peaks is found for the hybrids with increasing polymer MWs, together with more pronounced

0–0 and 0–1 vibronic absorption shoulders. The result indicates that the charge carriers and excitons in the higher MWP3HT can delocalize over a larger extent as a result of pie-pie stacking and a stronger wavefunction overlap. It is found that the transient photocurrent for the low MW sample is highly dispersive and the transit time t_{tr} can be estimated from the intersection point in the double-logarithmic plot (**Figure 2**). The increased carrier mobility with increased polymer MW is mainly attributed to the enhanced pie-electron delocalization and increased effective conjugation length in the main chain. Next, we fabricated the P3HT/TiO_2 nanorod hybrid photovoltaic devices by blending TiO_2 nanorods with different MW P3HT polymers. **Figure 3** shows the current–voltage (I–V) characteristic curves of the solar cells measured under AM 1.5 illumination. Compared to the low MW sample, the medium MW sample shows an improvement in the power conversion efficiency, accompanied by an increase in the short circuit current density (J_{sc}) by about 80%. The increased short circuit current in the medium sample is consistent with the result of enhanced carrier mobility with MW. For the high MW sample, large improvements in the fill factor and short circuit current are found. The improved fill factor may be attributed to the reduced serial resistance and increased carrier mobility as a result of enhanced electronic delocalization within polymer chains. In addition, the reason for the increase in V_{oc} for the high MW sample is not clear at the current stage, and one possible reason might be attributed to the reduction of back charge recombination rate at the P3HT/TiO_2 nanorod interfaces. The enhancement in the P3HT/TiO_2 nanorod hybrid photovoltaic performance by using higher MW P3HT is mainly attributed to enhanced pie-electron delocalization and more organized chain packing in the polymer, which shows good consistency with the observed redshift in the absorption spectra and increased mobilities with MWs.

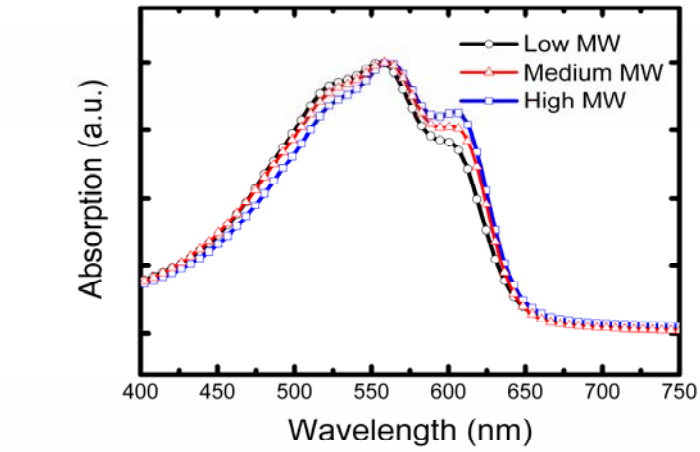

Figure 1 Normalized absorption spectra of P3HT/TiO_2 nanorod hybrids with different molecular weights.

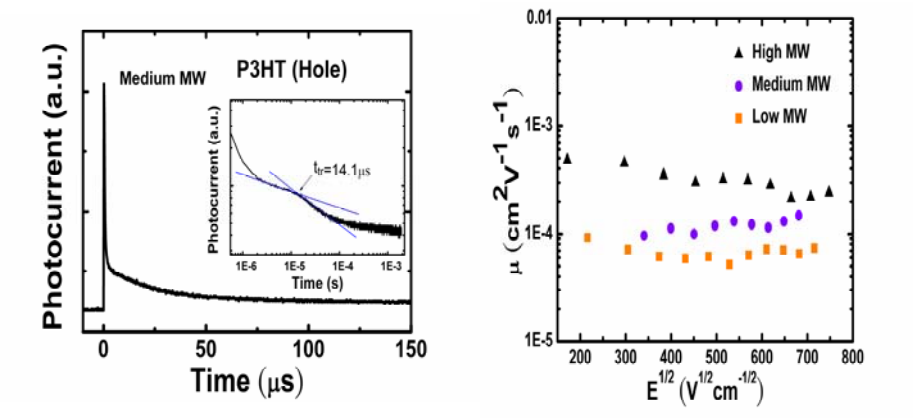

Figure 2 The TOF hole transient photocurrents for P3HT/TiO_2 nanorod hybrids with various molecular weight of P3HT. The insets show the double-logarithmic plots for the transient photocurrents.

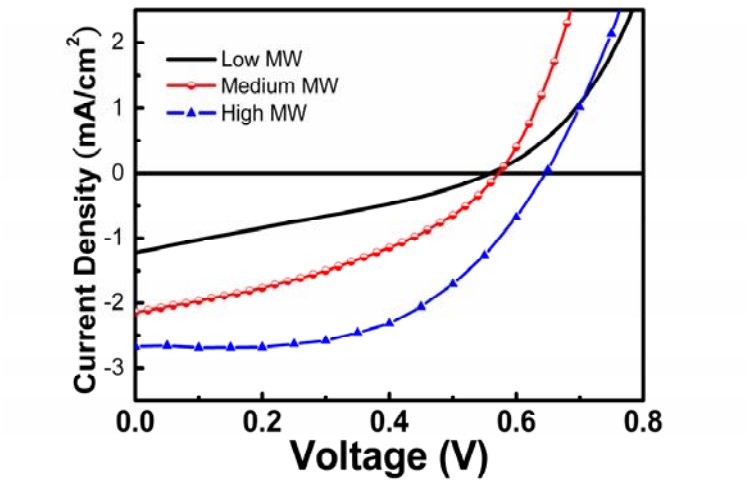

Figure 3 I–V characteristics of the photovoltaic devices based on P3HT/TiO_2 nanorod hybrids with different MW P3HT (under AM 1.5 illumination (100 mW cm^{-2})).

Since the device performance strongly depends on the film morphology, we further carried out the investigation of the nanoscale morphology by using SNOM and AFM. In the measurements, a SNOM probe with an aperture of around 100nm in diameter on the sharp end was placed into the near field of the investigated sample. High-quality optical contrast images were able to be obtained by this technique. In order to suppress the photoluminescence behavior of P3HT, simultaneous topography and absorption measurements were performed using a He–Ne laser of 632.8 nm wavelength. The surface topography and absorption contrast images of three P3HT/TiO_2 nanorod hybrid samples with different P3HT MWs are shown in **Figure 4**.

The results indicate that a larger extent of continuous absorption domains are formed in the samples with increasing MW, as a result of increased conjugation and delocalization. The nanoscale absorption images probed by SNOM provide direct information about the interplay between topography and absorption density in the polymer hybrid photovoltaic device application, since both the morphology and optical absorption of photovoltaic materials usually play crucial roles in determining the power conversion efficiency. We further used high resolution AFM to study the effect of polymer MW on the nanoscale morphology of P3HT/TiO_2 nanorod hybrid films as shown in **Figure 5**. The morphology and phase diagrams demonstrate that the rod-like structure is formed in the low MW hybrid sample while the high MW hybrid sample tends to form small nodule-like structure. The AFM data suggest that the rod-like structure of the low MW hybrid sample consists of a large amount of grain boundaries, which usually limit mobility and hinder carrier transport. In contrast, the nodule-like structure of the high MW hybrid sample shows less well-defined grain boundaries and a greater extent of continuous domains due to the increased conjugation as a result of enhanced polymer chain packing, which can improve the transport of charge carriers. In addition, the decrease in the number of grain boundaries and surface roughness for the P3HT/TiO_2 nanorod hybrid film with high polymer MW is also consistent with the observation of a more continuous absorption mapping image by SNOM measurement. In the data of the device performance in **Figure 3**, the observation of an increased V_{oc} in the high MW sample might be also attributed to the decreased number of grain boundaries, which can usually act as the recombination sites for carriers. The reduction of back charge recombination may increase the position of the quasi-Fermi level and V_{oc}. The nanoscale morphology of the hybrid samples with different MWs reveals the possible nature of the effect of polymer MWs on absorption, carrier transport and power conversion efficiency of P3HT/TiO_2 nanorod hybrid solar cells. We also conducted confocal Raman microscopic measurements to gain insight into the component distribution of the P3HT/TiO_2 nanorod hybrid sample (**Figure 6**). From the Raman mapping image, region I represents a TiO_2 rich region with strong TiO_2 vibrational signatures and region II represents a P3HT rich region with predominant P3HT vibrational signatures. No large extent of phase segregation as reported in the P3HT/PCBM hybrid was found in our P3HT/TiO_2 nanorod hybrid sample, which may result from the less mobile nature of TiO_2 nanorods compared to PCBM molecules.

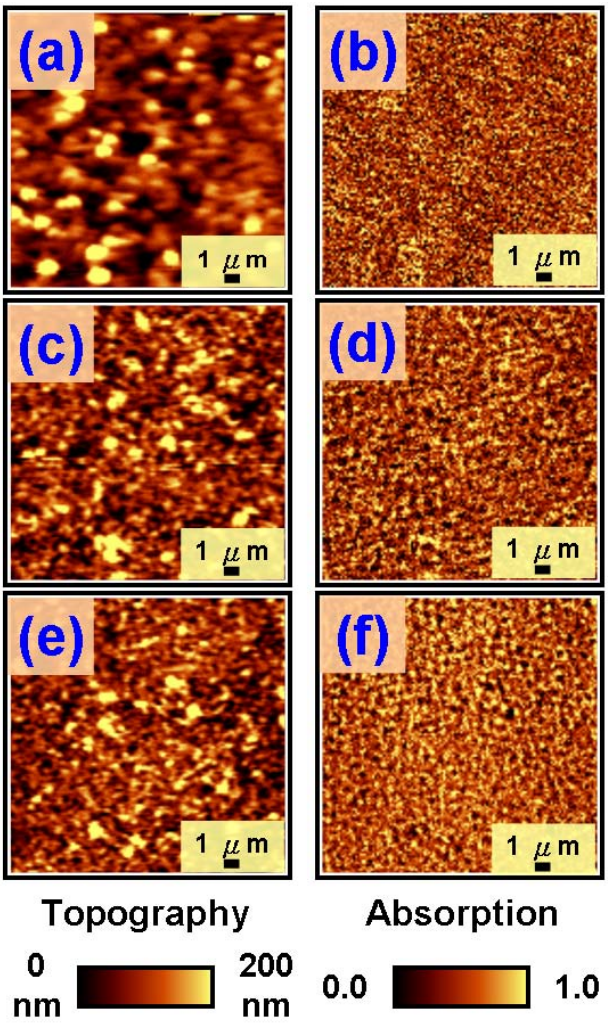

Figure 4 Topography (a,c,e) and optical contrast images (b,d,f) of P3HT/TiO_2 samples with three different P3HT molecular weights obtained in SNOM transmission mode using laser radiation with 632.8 nm wavelength.The MWs in the P3HT/TiO_2 nanorod hybrid samples are low MW for (a,b), medium MW for (c,d) and high MW for (e,f). The scan size is 20 nm x20 nm.

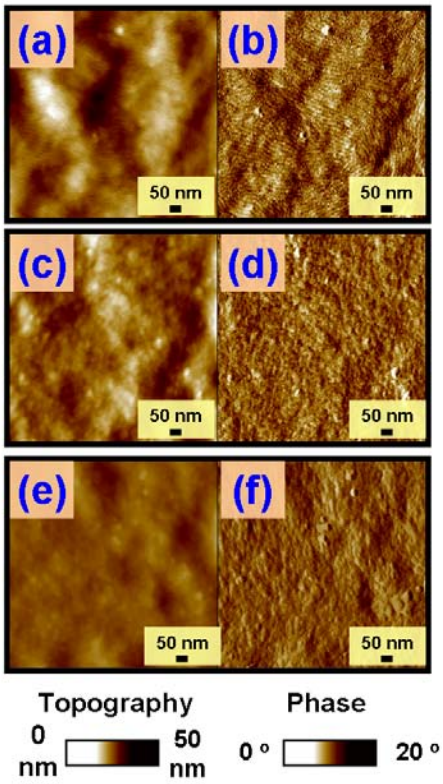

Figure 5 Topography (a,c,e) and phase images (b,d,f) of P3HT/TiO_2 nanorod hybrid samples with three kinds of P3HT MWs obtained in AFM tapping mode, scan size is 2 mm_ 2 mm. Images (a,b) were obtained from the low MW sample of P3HT/TiO_2 nanorod hybrid; (c,d) were obtained from the medium MW sample; (e,f) were obtained from the high MW sample.

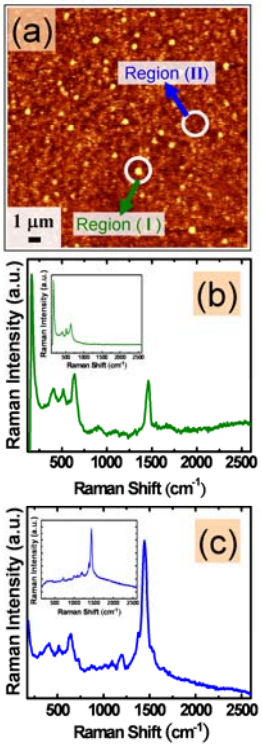

Figure 6 (a) Confocal Raman mapping image of the P3HT/TiO_2 nanorod hybrid sample with high MW. Images (b) and (c) show the corresponding Raman shift spectra resulting from different selected areas (regions I and II) respectively. The Raman shift spectra for TiO_2 and pristine P3HT are also shown in the insets of (b) and (c) respectively.

In summary, we have performed the nanoscale investigation of the effect of polymer MW on the performance of photovoltaic devices based on P3HT/TiO_2 nanorod hybrid materials. From the data measured by SNOM and AFM, a more continuous absorption region and a reduction in the number of grain boundaries for the high MW P3HT/TiO_2 nanorod hybrid film can be obtained due to enhanced electronic delocalization. The confocal Raman mapping images also provide information for the component distribution in the hybrids. The results provide a direct observation of the correlation between the nanoscale absorption, morphology and device performance in P3HT/TiO_2 nanorod hybrid solar cells.

Improved performance of polymer/TiO_2 nanorods bulk heterojunction photovoltaic devices by interface modification[14,15]

TiO_2 nanorods have a dimension of 20-40 nm in length and 4-5nm in diameter as was revealed by the HRTEM image in **Figure 7**(a). Typically, the as-synthesized TiO_2

nanorods are capped with insulating surfactant of oleic acid (O.A.) consisting of a long alkyl chain, which may act as a potential barrier for charge transfer. We therefore carried out the interface modification to replace the original oleic acid ligand using two different kinds of ligand molecules, i.e. pyridine (Pyr.) and cis-bis (4,4-dicarboxy-2,2-bipyridine) dithiocyanato ruthenium(II) (N3 dye) respectively. The three different kinds of surface ligands are shown schematically in **Figure 7**(b).

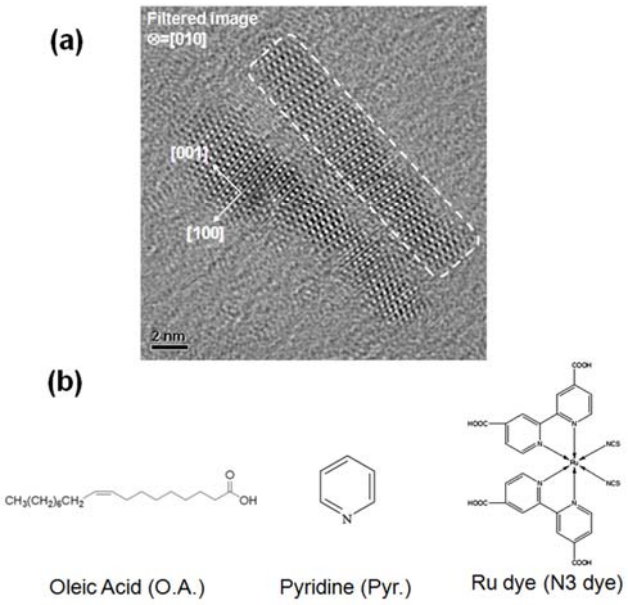

Figure 7 High-resolution transmission electron microscopy (HRTEM) image of TiO_2 nanorods used in this work. TiO_2 nanorods were capped by O.A. originally but were replaced by Pyr. and N3 dye in the following process.

The current-voltage characteristics of the devices with different configurations under simulated A.M. 1.5 illumination are shown in **Figure 8**. The device based on the P3HT:TiO_2 nanorods (O.A.) hybrid material exhibits a short circuit current density (J_{sc}) of 1.67 mA/cm^2, an open circuit voltage (V_{oc}) of 0.65 V, and a fill factor (FF) of 0.35, resulting in a power conversion efficiency (η) of 0.38 %. For the device based on the hybrid with TiO_2 nanorods by pyridine treatment, a large increase in the fill factor indicates that removal of insulating surfactant on the TiO_2 nanorods results in a significant improvement in the serial resistance of the device. The performance of the device based on the P3HT:TiO_2 nanorods (PYR) hybrid material exhibits a short circuit current density (J_{sc}) of 2.61 mA/cm^2, an open circuit voltage (V_{oc}) of 0.69 V, and a fill factor (FF) of 0.62, resulting in a power conversion efficiency (η) of 1.12 %. For the device consisting of TiO_2 nanorods modified by the N3 dye molecule, a further improvement in the device performance is found, giving a short circuit current density (J_{sc}) of 4.33 mA/cm^2, an open circuit voltage (V_{oc}) of 0.78 V, and a fill factor

(FF) of 0.65, resulting in a power conversion efficiency (η) of 2.20 %. It is worth noting that the amount of adsorbed N3 dye on TiO_2 nanorod surface is estimated to be low about $1.3x10^{-12}$ mole/cm^2 of TiO_2 nanorod and a negligible optical density of interface layers of these molecules in relation to that of P3HT was also found. This result indicates that these ligand molecules modify the interface rather than harvest light.

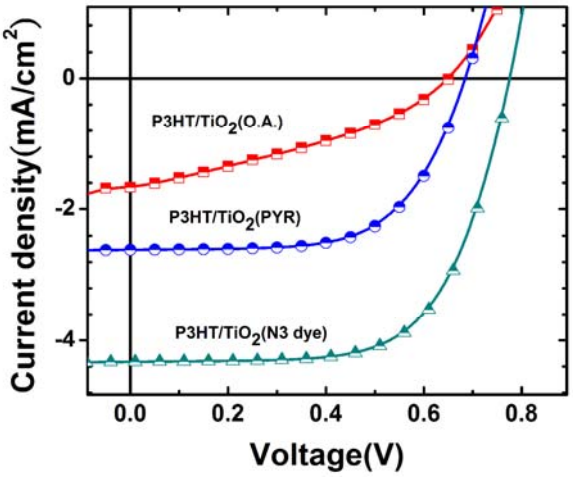

Figure 8 Current – voltage characteristics of P3HT/TiO_2 BHJ solar cells using different interface ligand molecules under A.M. 1.5 (100mW/cm^2) irradiation.

The interfacial molecules can (i) facilitate charge separation or (ii) prevent back recombination at the interfaces of P3HT/TiO_2 nanorod hybrids. Time-resolved photoluminescence spectroscopy (TRPL) and transient open-circuit voltage decay (TOCVD) measurements were performed to examine the two types of carrier dynamics in hybrids after interface modification. **Figure 9**(a) shows the photoluminescence of P3HT/TiO_2 hybrids and suggests the occurrence of PL quenching from charge separation. The PL quenching efficiency *Q* for the three samples is $Q_{N3} > Q_{Pyr.} > Q_{O.A.}$, indicating that more efficient charge separation can be achieved at the P3HT/TiO_2 nanorods interfaces by either removing the insulating surfactant or replacing it with a more conductive ligand. The improved charge separation efficiency at the P3HT/TiO_2 nanorods interfaces can also be inferred from TRPL spectroscopy. **Figure 9**(b) shows the PL decay curves for the pristine P3HT and the hybrid films with different surface modification respectively. The addition of TiO_2 nanorods in polymer results in a new relaxation process, which provides to the donor a further non-radiative process and leads to shortening of the measured lifetime τ. The measured PL lifetime for the pristine P3HT and P3HT/TiO_2 nanorods hybrid with

O.A., PYR and N3 surfactant areτ_{P3HT}=676ps, τ_{OA}=480ps, τ_{PYR}=255ps, and τ_{N3}=232ps, respectively, indicating that more efficient charge separation takes place at the polymer/TiO_2 nanorods interfaces by removing the insulating ligand O.A. or replacing with a more conductive ligand of Pyr. and N3 dye, consistent with the PL quenching result.

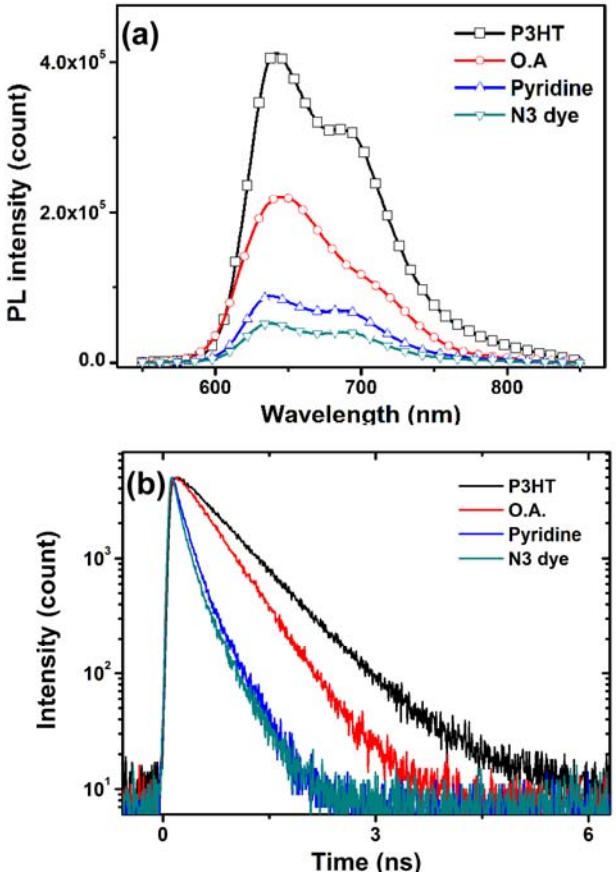

Figure 9 (a) PL spectrum and (b) TRPL spectroscopy of P3HT/TiO_2 nanorod hybrids following different interface modifications.

However, the effect of enhanced charge separation efficiency alone can not account for the significant improvement in both J_{sc} and V_{oc} of devices upon interface modification. Accordingly, transient open-circuit voltage decay (TOCVD) measurements were performed to determine the recombination rate at the interfaces between polymer and TiO_2 nanorods in an operating solar cell device under an open circuit condition. A small perturbation generated by a pulsed laser produces extra electrons and holes in hybrids. The decay of the photovoltage that is generated by the additional carriers from the small perturbation corresponds to the recombination rate at the heterojunctions. **Figure 10** plots the charge recombination rate constant

k_{rec} versus illumination intensity under open circuit conditions. The recombination rates k_{rec} follow the order O.A. capped sample > pyridine modified sample > N3 dye modified samples at all light intensities, showing a good consistence with the photovoltaic performance. The interface modifier of the N3 dye molecule acts as the most effective recombination barrier with respect to other ligand molecules. As described above, the reduced recombination rate may lead to increased electron and hole concentrations at interfaces, increasing the difference between the quasi-Fermi levels of electrons and holes, and accounting for the observed increase in V_{oc} upon interface modifications. Furthermore, the suppression of back recombination at the interfaces can increase the number of carriers that can be transported toward electrodes, as a result of improved J_{sc} after interface modification. From the above result, it is concluded that interface modifications on the TiO_2 nanorod surface can be used to significantly improve the device's performance by enhancing charge separation, while strongly suppressing back recombination which take place at P3HT and TiO_2 heterojunctions.

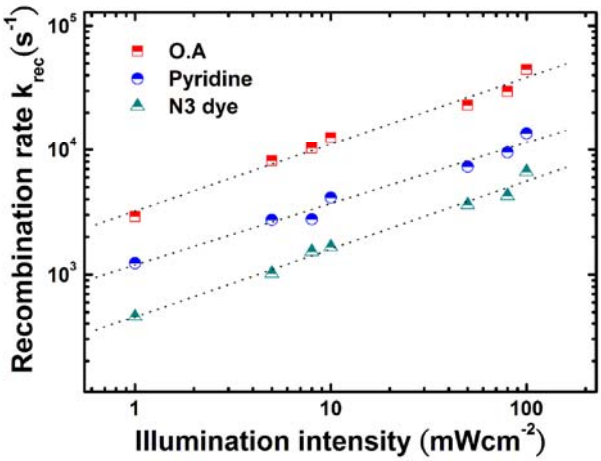

Figure 10 Charge recombination rate constant *krec* versus light intensity at open circuit voltage determined by TOCVD measurement

Improved performance of polymer/TiO_2 nanocrystals hybrid solar cell by fluorine-doped TiO_2

In the photoluminescence spectrum (**Figure 11**), the peak positions of the doped and undoped one are both at about 510 nm, showing no significant shift in the PL spectrum after doping. The difference between the absorption edge (380 nm, 3.26 ev)

and the emission peak energy (510 nm, 2.43 ev) can be attributed to the stoke-shift caused by the Frank-Condon effect. An obvious difference of PL intensity can be seen between the doped and undoped TiO_2. The lower intensity of the F-doped TiO_2 may originate from the reduction of band-to-band recombination. The fluorine doping would introduce Ti^{3+} surface states by charge compensation and create intra-band donor levels closely below the conduction band since TiO_2 is intrinsic n-type semiconductor material.

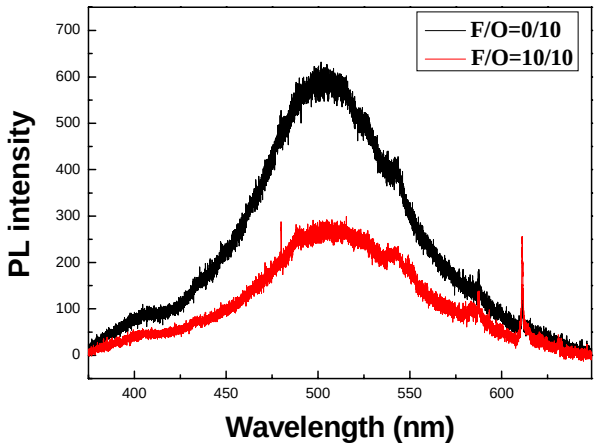

Figure 11 Photoluminescence spectra of doped and undoped TiO_2 nanocrystals

Figure 12 shows the dark I-V curve and **Figure 13** shows the I-V curve under AM1.5 irradiation of the photovoltaic devices using different doping concentration in the TiO_2 nanoparticles. From the dark I-V curve, a clear decrease in the turn on voltage and series resistance can be observed for the higher doping-concentration TiO_2/P3HT hybrid solar cells, showing higher electrical conductivity in these photovoltaic devices. The fill factor and efficiency of these devices are enhanced as we doping fluorine atoms into the TiO_2. The device performance may be further improved beyond the highest efficiency of TiO_2/P3HT system (2.2%) nowadays by surface modification of the F-doped TiO_2 nanoparticles and adding hole-block layer on top of the active layer, in which both procedures haven't been taken in our device fabrication this time. Interestingly, the J_{sc} increases while the V_{oc} decreases as we enhance the doping concentration.

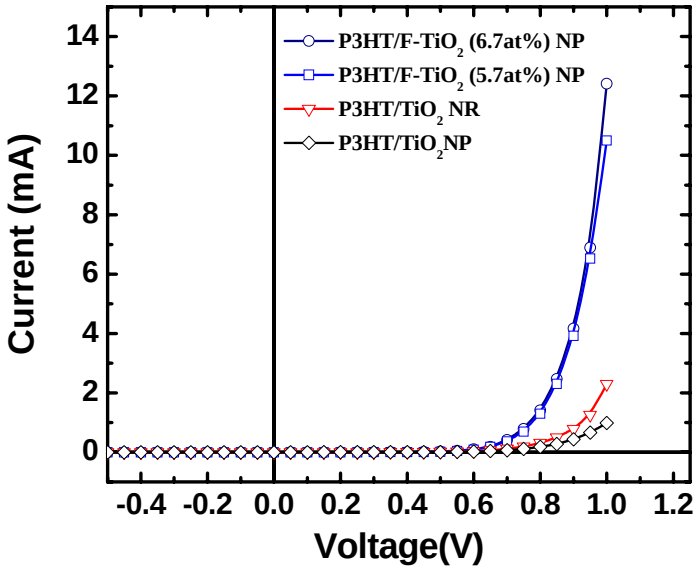

Figure 12 Dark I-V curve of F-doped TiO_2/P3HT photovoltaic device.

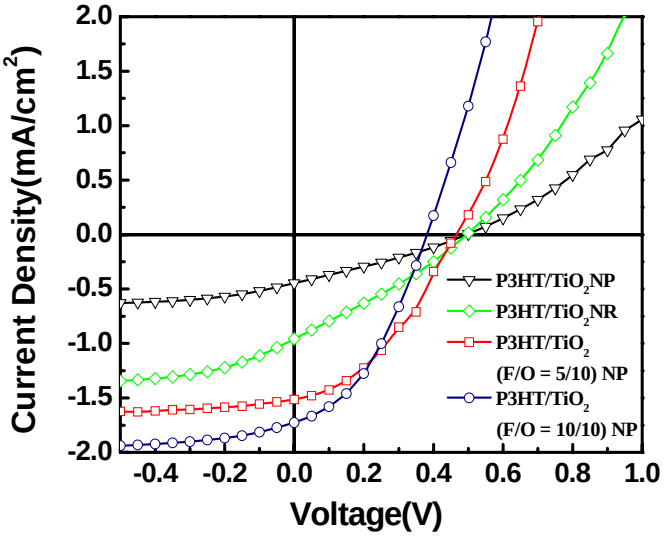

Figure 13 I-V curve of F-doped TiO_2/P3HT photovoltaic device under AM1.5 illumination.

The enhancement of photocurrent with increased doping concentration is understandable since fluorine-doping in TiO_2 would increase carrier concentration and reduce the recombination rate, which is quite consistent with our original purposes, but the reduction of open circuit voltage is beyond our expectation. Since the typical photocarrier concentration (10^{15}~10^{16}/cm^3) is smaller than the DOS at valence band

edge and conduction band edge, the V_{oc}, which is the gap of electron quasi-Fermi (E_{FN}) levels and hole quasi-Fermi level (E_{FP}) under illumination, is limited by the Ec-HOMO gap. The preliminary explanation of the phenomenal of decreased V_{oc} is the problem of Fermi-level pinning caused by the defect sites of doped nanocrystals. As Fermi-level pinning happened, lots of photocarriers would be trapped into the defect site in the nanocrystals and Fermi-level from TiO_2 would shift downward, resulting in lower gap between electron quasi-Fermi (E_{FN}) levels and hole quasi-Fermi level (E_{FP}) under AM1.5 illumination, that is, the lower V_{oc} for the photovoltaic device. The **Figure 14** below shows the as-proposed mechanism:

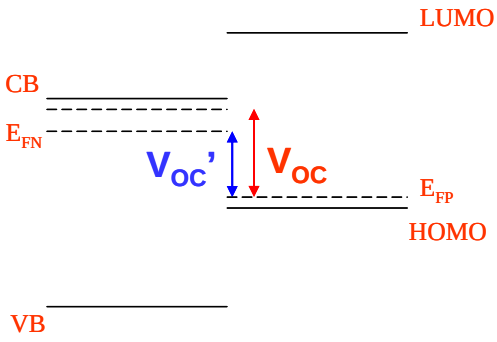

Figure 14 Proposed mechanism explaining the decreased open-circuit voltage

Optoelectronic Properties and Electrochemical Properties of Alternating Fluorene-Cyclopentadithiophene Copolymers[16]

The synthetic routes of monomers are outlined in **Scheme 1**. The polymerization reactions as shown in **Scheme 2** were based on the palladium catalyzed Suzuki coupling reaction and carried out in a mixture of toluene and aqueous potassium carbonate solution (2 M) containing 1 mol % [$Pd(PPh_3)_4$] under vigorous stirring and refluxed at 115°C for 48 h under nitrogen. Poly-{2,6-(4*H*-cyclopenta[2,1-b:3,4-b']dithiophene)-2,7-(9,9-dihexylfluorene)} (**P1**), poly-{2,6-(4,4-ethylenedioxy-4*H*-cyclopenta[2,1-b:3,4-b']dithiophene)-2,7-(9,9-dihexylfluorene)} (**P2**), poly-{2,6-(4,4-propylenedioxy-4*H*-cyclopenta[2,1-b:3,4-b']dithiophene)-2,7-(9,9-dihexylfluorene)} (**P3**), poly-{2,6-(4*H*-cyclopenta[2,1-b:3,4-b']dithiophen-4-one)-2,7-(9,9-dihexylfluorene)} (**P4**), and poly-{2,6-(4-ylide-nemalononitrile-4*H*-cyclopenta[2,1-b:3,4-b']dithiophene)-2,7-(9,9-dihexyl-fluorene)} (**P5**) were prepared in very good yields (57-93%). **P4** can be synthesized also by the hydrolysis of **P2** with concentrated HCl in THF with a yield

of 96%. **P4** can be further reacted with malononitrile in THF to obtain **P5** in 59% yield. After purification and drying the polymers **P1**, **P2**, **P3**, **P4** and **P5** were obtained as brown solid, brownish green solid, brownish black solid, deep green solid and deep brown solid powders respectively. All these polymers are readily soluble in common organic solvents such as THF, chloroform, toluene and xylene. The chemical structures of the monomers and polymers were confirmed by ^{1}H NMR, ^{13}C NMR and FTIR spectra. The major signal of ^{1}H NMR spectra of **P1**-**P5** at δ 7.43, δ 7.27, δ 7.25, δ 7.30 and δ 8.62 can be assigned to the proton at position 3 on the cyclopentadithiophene ring. The specific signal of **P1** at δ 3.61 can be assigned to methylene protons at position 4 on the cyclopentadithiophene ring. The specific peak of **P2** at δ 4.41 can be assigned to four ethylenedioxy protons at position 4 and the peaks at δ 4.39 and δ 2.15 of **P3** can be assigned to six propylenedioxy protons at position 4 on the cyclopentadithiophene ring. The ^{13}C NMR signal of **P4** at δ 182.00 can be assigned to position 4 keto group (C=O) on the cyclopentadithiophene ring. The FTIR spectra show **P4** film has a strong band of carbonyl group (C=O stretching mode) at 1707 cm^{-1} and also **P5** film exhibits the strong bands of the cyano group (CN stretching mode) at 2190 cm^{-1} and 2174 cm^{-1}. All NMR spectra of copolymers are shifted to downfield as compared to their monomer spectra due to the polymerization.

Scheme 1 Synthetic Routes for Monomers[a]

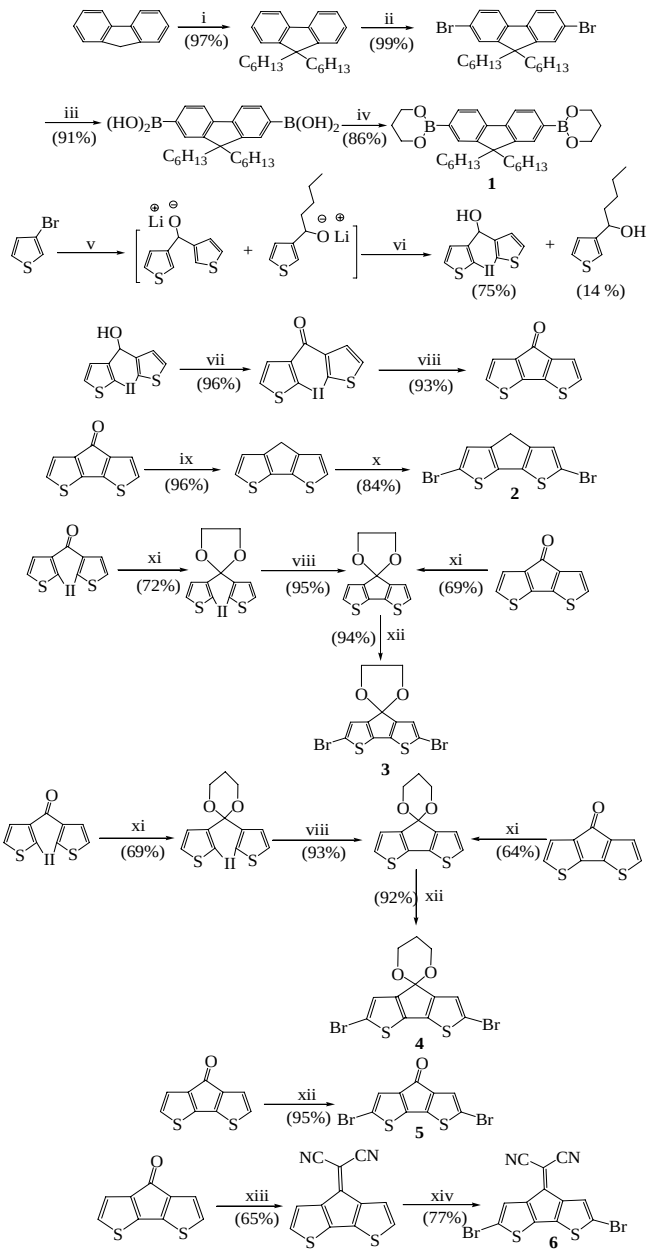

[a]Reagents and Conditions: i.THF, n-BuLi, $C_6H_{13}Br$, -78°C, ii. $CHCl_3$, $FeCl_3$ (cat.), Br_2, iii. THF, n-BuLi, $B(OBu)_3$, -78°C, 2 M HCl, iv. Toluene, 1,3-propandiol, Reflux, v. (a) Ether, n-BuLi-78°C, (b) 3-thiophenecarboxaldehyde, vi. (a) n-BuLi (2eqiv.), -23°C, I_2 (3eqiv.), (b) Na_2SO_3 and HI solu[n], vii. CH_2Cl_2, P.C.C, r.t, viii. Cu, DMF, Reflux, ix. $HOCH_2CH_2OH$, $NH_2NH_2.H_2O$, KOH, 180°C, 18h., x. $CHCl_3$, $FeCl_3$ (cat.), Br_2, xi. C_6H_6, $HOCH_2CH_2OH$, PTSA (cat.), azeotrope, 110°C, 4 days, xii. THF, NBS, 0°C, 1h, xiii. THF, $CH_2(CN)_2$, Piperidine (cat.), Reflux, 14h, xiv. DMF, NBS, 5h.

Scheme 2 Synthetic Routes for Polymers[a]

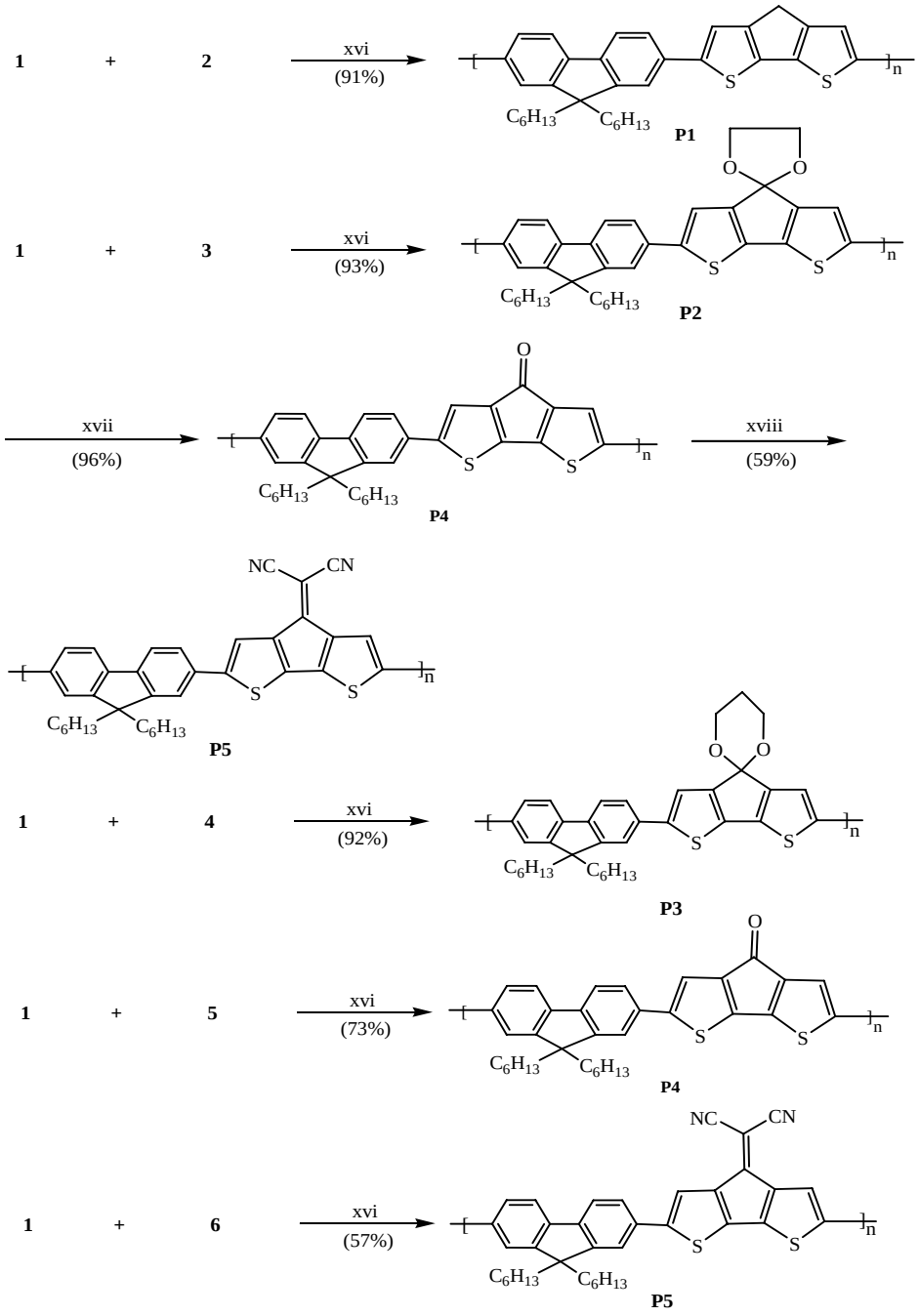

[a]Reagents and Conditions: xvi. $[(PPh_3)_4]Pd(0)$ (1.0 Mol %), Toluene/2 M K_2CO_3 (3:2), Reflux, 115^oC, 48h, xvii. THF, Conc^n HCl, 1h, xviii. THF, $CH_2(CN)_2$, Piperidine (cat.), Reflux, 14h.

Optical Properties. Table 1 summaries the UV and PL spectra of copolymers **P1**-**P5.** In solution, compared to **P1**, **P2** and **P3** exhibited red-shifted spectra with $\Delta\lambda_{abs}$ = 26-29 nm and $\Delta\lambda_{fl}$ = 16 nm respectively. The spectral shifts could be attributed to the spiro connection of the 4,4-ethylenedioxy and 4,4-propylenedioxy groups with the conjugated polymer backbone so that the lone pairs of the oxygen atoms might have certain orbital interactions with the π-electrons of the polymer backbone. Such kind of orbital interactions enables the oxygen atoms serve as electron donating groups to effectively lower the HOMO and thus to reduce the band gap. In contrast, the absorption maxima for **P4** and **P5** are blue shifted along with a shoulder (**P5**) or weak band (**P4**) in the red edge. Apparently, the $S_0 \rightarrow S_1$ transition becomes less allowed. These phenomena are reminiscent of the *meta* conjugation effect observed for aminostilbenes. In other words, the electronic interaction between the π-substitutents, carbonyl and dicyanoethenyl groups, and the π-conjugated polymer backbone resembles the case of *meta*-phenylene bridged subunits. The weak fluorescence of **P4** and **P5** is also consistent with the forbidden nature of optical transition between S_0 and S_1. Similar spectral properties are also observed for **P1**-**P5** in thin solid films. It is particularly interesting to note that the fluorescence maxima (508 nm) of **P4** is blue-shifted with respect to its $S_0 \rightarrow S_1$ absorption band (586 nm), which appears to indicate that the fluorescence is mainly from the $S_2 \rightarrow S_0$ transition. We have used the intersection point of UV-vis and fluorescence spectra of **P1**-**P5** thin films to estimate the band gap (E_g) of the polymers. The **P2**, **P3** exhibit a lower band gap than that of **P1** due to the spiro connection of the 4,4-ethylenedioxy and 4,4-propylenedioxy groups with the conjugated polymer backbone. The **P4** and **P5** exhibit a higher band gap than that of **P1** due to the *meta* conjugation effect to prevent the π-electron delocalization by carbonyl and dicyanoethenyl groups (**Table 1**).

Table 1 Optical properties of fluorene cyclopentadithiophene copolymers

Polymer	UV-vis in THF sol^n λ_{max} (nm)	PL in THF sol^n λ_{max} (nm)	Φ_{fl}	UV-vis in films λ_{max} (nm)	PL in films λ_{max} (nm)	Wavelength of intersection point of UV-vis and PL	E_g (eV)
P1	443	516	0.40	438	523	498	2.49
P2	469	532	0.41	467	554	519	2.39
P3	472	532	0.42	484	564	539	2.30
P4	394, 586	508	<0.01	395, 589	508	649 479	2.59, 1.91
P5	353	498	0.06	345	509	484	2.56

Electrochemical Properties. Cyclic voltammetry (CV) experiments were conducted to probe the electrochemical properties of **P1**-**P5**. The voltammograms and the onset potentials of oxidation ($E_{onset, ox}$) and reduction ($E_{onset, red}$) are summarized in **Table 2**. All measurements were calibrated using ferrocene (Fc) value of +0.32 eV as the standard. The HOMO and LUMO and thus the electrochemical band gaps, $E_g = (E_{LUMO} - E_{HOMO})$, could be estimated (**Table 2**) according to the empirical relationship proposed by de Leeuw et al (eq 1):

I_p (HOMO) = -($E_{onset, ox}$ + 4.39) (eV), E_a (LUMO) = -($E_{onset, red}$ + 4.39) (eV) eq 1

The resulting band gaps are slightly higher than the optical bandgap (see **Table 2**) for **P1**, **P4** and **P5** due to interface barrier for charge injection. However, the electrochemical band gaps of polymers **P2** and **P3** are smaller than that measured from the UV-vis spectrum, because the oxidation potential of these two polymers could not be measured exactly. It should be noted that incorporation of the electron-deficient fluorene derivative into the polycyclopentadithiophene backbone decreases the energy level of HOMO but increases that of LUMO, leading to a higher band gap in the copolymers (**P4**: 2.11 eV) versus the cyclopentadithiophene homopolymer (1.70 eV).

Table 2 Electrochemical properties and energy levels of fluorene cyclopeantadi-thiophene copolymers

polymer	$E_{Onset.Oxd}$ (eV)	$E_{Onset.Red}$ (eV)	HOMO (eV)	LUMO (eV)	E_g (eV)
P1	1.74	-0.82	6.13	3.57	2.56
P2	1.40	-0.90	5.79	3.49	2.30
P3	0.96	-0.86	5.35	3.53	1.82
P4	1.08	-1.03	5.47	3.36	2.11
P5	1.75	-0.96	6.14	3.43	2.71

Conclusions

We have fabricated polymer/inorganic nanocrystals hybrid solar cells based on P3HT/TiO_2 nanorods bulk heterojunction hybrids. The device performance is largely dependent on nano morphology of polymer/nanocrystal hybrid. In addition, by interface modification with effective molecules, the photovoltaic performance in both device structures can be largely improved due to enhanced charge separation and suppressed interface recombination rate in the polymer/inorganic hybrids. New materials F-doped TiO_2 and alternating copolymers of fluorine and cyclopentadithiophene derivatives were synthesized and characterized. They are expected to further improve the cell efficiency.

References

1. W. U. Huynh, J. J. Dittmer, and A. P. Alivisatos, **2002**, *Science*, 295, 2425.
2. W. Ma, C. Yang, X. Gong, K. Lee, and A. J. Heeger, **2005**, *Adv. Func. Mater.* , 15, 1617.
3. R. H. Friend, G. J. Denton, J. J. M. Halls, N. T. Harrison, A.B. Holmes, A. Kohler, A. Lux, S. C. Moratti, K. Pichler, N. Tessler, K. Towns, H. F. Wittmann, **1997**, *Solid State Commun.*, 102, 249.
4. T. J.Savenije, J. M. Warman, and A. Goossens, **1998**, *Chem. Phys. Lett*., 287, 148.
5. A. C. Arango, L. R. Johnson, V. N. Bliznyuk, Z. Schlesinger, S. A. Carter, and H. H. Horhold, **2000**, *Adv. Mater.,* 12, 1689.
6. G. Yu and A. J. Heeger, **2001,** *J. Appl. Phys.*, 78, 4510.

7. Haugeneder, M. Neges, C. Kallinger, W. Spirkl, U. Lemmer, and J. Felmann, **1999**, *Phys. Rev. B*, 59, 15346.
8. N. C. Greenham, X. Peng, and A. P. Alivisatos, **1996**, *Phys. Rev. B*, 54, 17628.
9. J. S. Salafsky, **1999**, *Phys. Rev. B*, 59, 10885.
10. P. A. van Hal, M.M. Wienk, J. M. Kroon, W. J. H. Verhees, L. H. Slooff, W. J. H. van Gennip, P. Jonkheijm, and R.A.J. Janssen, **2003**, *Adv. Mater.*, 15, 118.
11. C. Y. Kwong, W. C. H. Choy, A. B. Djurisic, P. C. Chui, K. W. Cheng, and W. K. Chan, **2004**, *Nanotechnology*, 15, 1156.
12. Ming-Chung Wu, Yi-Jen Wu, Yu-Ching Huang, Chih-Min Chuang, Kuo-Chung Cheng, Ching-Fuh Lin, Yang-Fang Chen and Wei-Fang Su, "Surface Potential and Magnetic Properties of $La_{0.7}Sr_{0.3}MnO_3$ Periodic Arrays Fabricated by Direct Electron Beam Writing," **2008,** *Journal of Applied Physics*, 104, 024517.
13. Ming-Chung Wu, Hsueh-Chung Liao, Hsi-Hsing Lo, Sharon Chen, Yun-Yue Lin, Wei-Che Yen, Tsung-Wei Zeng, Chun-Wei Chen, Yang-Fang Chen and Wei-Fang Su, "Nanostructured Polymer Blends (P3ht/Pmma): Inorganic Titania Hybrid Photovoltaic Devices," **2009**, *Solar Energy Materials and Solar Cells*, 93, 961-965.
14. Yun-Yue Lin, Shao-Sian Li, Tsung-Hung Chu, Chia-Hao Chuang,Chia-Hao Chang,Wei-Fang Su, Ching-Pin Chang, Ming-Wen Chu and Chun-Wei Chen, "Interfacial nanostructuring on the performance of polymer/TiO_2 nanorod bulk heterojunction solar cells," **2009**, *Journal of American Chemical Society, (JACS)*, 131, 3644.
15. Shao-Shen Li, Yun-Yue Lin, Wei-Fang Su and Chun-Wei Chen, "Polymer/metal oxide hybrid solar cells", **2009**, *IEEE Journal of Selected Topics in Quantum Electronics*: "Next-Generation Organic and Hybrid Solar Cells", (Invited), (accepted)
16. Bikash Pal, Wei-Che Yen, Jye-Shane Yang, Chi-Yang Chao, Ying-Chieh Hung, Shiang-Tai Lin, Chia-Hao Chuang, Chun-Wei Chen and Wei-Fang Su, "Substituent Effect on the Optoelectronic Properties of Alternating Fluorene-Cyclopentadithiophene Copolymers," **2008**, *Macromolecules*, 41, 6664-6671.